A topographic test for the existence of ground ice in the walls of Coprates Chasma, Mars

Jørn Atle Jernsletten
Seabrook, Texas, USA

Received 29 March 2004; revised 5 August 2004; accepted 18 August 2004; published 15 December 2004.

[1] Evidence for the former presence of ground ice and its possible role in the erosion of Valles Marineris trough walls is equivocal. This study aims to determine whether variations in the topographic slope angle of the walls of the trough Coprates Chasma are consistent with predicted temperature-driven differences in the distribution, thermal condition, and strength of ground ice within its walls. Using Mars Orbiter Laser Altimeter topographic data, 247 profiles were made rim to rim across the trough and measurements made of wall slope angle, mean annual surface temperature, and trough geometry (wall height, rim elevation, and trough width). Variations in these parameters along each trough wall, and differences between the two trough walls, were established. The results indicate that the predicted variations along and differences between the walls in the three-dimensional distribution of ground ice, and in its thermal condition and strength, are unlikely to have caused the measured variations in trough wall slope angle. These observations imply that ground ice has been absent within the trough walls since the age of formation of the spur-and-gully wall morphology. The results preclude the spur-and-gully morphology having developed by dry mass-wasting of material above an ice-rich cryosphere and indicate the action of liquid water to be a more likely origin. The inferred absence of ice within the walls precludes any role of ice in initiating or mobilizing landslides where they have eroded the spur-and-gully morphology. *INDEX TERMS:* 5470 Planetology: Solid Surface Planets: Surface materials and properties; 5460 Planetology: Solid Surface Planets: Physical properties of materials; 5416 Planetology: Solid Surface Planets: Glaciation; 5415 Planetology: Solid Surface Planets: Erosion and weathering; 5464 Planetology: Solid Surface Planets: Remote sensing; *KEYWORDS:* Coprates Chasma, ground ice, Mars

Citation: Jernsletten, J. A. (2004), A topographic test for the existence of ground ice in the walls of Coprates Chasma, Mars, *J. Geophys. Res.*, *109*, E12004, doi:10.1029/2004JE002272.

1. Introduction

[2] Valles Marineris is a system of large troughs in the equatorial region of Mars that extends for over 4,000 km from west to east, with individual troughs measuring up to 11 km deep, 250 km wide, and over 1,000 km long. Many processes have been hypothesized to explain various aspects of the formation and geometry of the troughs, including tectonic, collapse, and erosional mechanisms [e.g., *Sharp*, 1973; *Blasius et al.*, 1977; *McCauley*, 1978; *Tanaka and Golombek*, 1988; *Schultz*, 1991]. One of the outstanding questions concerning the evolution of Valles Marineris troughs, and of equatorial features in general, concerns the possible past or current presence of volatiles (particularly water/ice) in the near-surface crust and their role in erosional processes [*Lucchitta*, 1979, 1987; *Rossbacher and Judson*, 1981; *McEwen*, 1989; *Davis and Golombek*, 1990; *Clifford*, 1993; *Peulvast et al.*, 2001].

[3] This study examines the possibility that topographic patterns in the trough walls of Coprates Chasma, the deepest and longest of the troughs, may reflect the differential presence of ground ice within the walls. The premise of the study is that surface heat variations caused by differences in aspect between the north and south walls of the trough, and by variations in latitude along them, may have generated topographic asymmetries between the walls. This premise is based on the notion that, over geologically significant periods of time, surface heat variations have affected the strength of slope-forming material via the temperature dependence of ice and of ice-related processes in the wall material. Because Coprates Chasma is located in the southern hemisphere of Mars, the south walls should be warmer than the north walls given the theoretical differential in solar incidence.

[4] Although near-surface ground ice does not currently exist in equatorial regions [*Leighton and Murray*, 1966; *Fanale*, 1976; *Farmer and Doms*, 1979; *Boynton et al.*, 2002; *Feldman et al.*, 2002], various geomorphic features have been interpreted in terms of the former existence of ground ice. Features with flow-like morphologies similar to those of terrestrial rock glaciers have been observed in the Valles Marineris region [*Rossi et al.*, 2000]. Onset diameters of rampart craters whose ejecta blankets may represent

0148-0227/04/2004JE002272$09.00

material mobilized by melted ground ice during impact [*Costard*, 1989; *Kuzmin et al.*, 1988a, 1988b; *Squyres et al.*, 1992] are greatest near the equator and least at latitudes of 50–60°. From such data, *Kuzmin et al.* [1988a, 1988b] estimated the depths to ground ice as being ~400 m at the equator and ~250 m at 30° latitude. However, *Clifford* [2003] has argued that surface features are not necessarily reliable indicators of either the past or present existence of ground ice in equatorial (or other) regions, as geomorphic interpretations are ambiguous and the ages of such features are largely unknown.

[5] Many processes with confirmed, or suspected, roles in Martian landscape evolution are known to be temperature-dependent, with many of these related to the hypothesized presence of ground ice. Suspected temperature-dependent physical and weathering processes on Mars include frost riving, oxidation, hydration, and carbonation [*Gooding et al.*, 1992]. Postulated temperature-dependent slope processes include the creep of rock/ice regolith, the growth and creep of ice-filled rock joints, the formation and movement of rock glaciers and debris flows, and the initiation and flow behavior of landslides [*Squyres*, 1978; *Carr*, 1981; *Squyres*, 1989; *Lucchitta et al.*, 1992; *Whalley and Azizi*, 2003]. Sublimation of ground ice, a temperature-dependent process, has occurred in the equatorial regions in the past [*Clifford and Hillel*, 1983], and may have influenced the erodability of slope-forming host materials [*Peulvast et al.*, 2001].

[6] The ways in which these processes operate are, to a large degree, understood through the quantified understanding of Earth analogs. Laboratory experiments show that the temperature dependence of the strength of ice yields a steady state strain rate during steady state creep that decreases by a factor of 20 for a 20 K (10%) drop in temperature from 240 to 220 K [*Durham et al.*, 1992]. When ice fills most of the pore space in frozen ground, the mechanical properties and behavior of frozen ground correspond closely to those of ice [*Andersland and Ladanyi*, 1994], with temperature influencing the mechanical properties in three ways. First, temperature is the main factor in determining the fraction of water in the ground that is ice. Second, the internal bonds in ice become stronger with lower temperatures. And third, at lower temperatures, an incremental increase in stress results in less thawing and a slower rate of water migration, which are important factors in stress redistribution [*Williams and Smith*, 1989]. These factors combine to make frozen ground stronger at lower temperatures [*Tsytovich*, 1960; *Sayles*, 1966; *Bourbonnais and Ladanyi*, 1985a, 1985b].

[7] Given that variations in insolation (resulting from aspect or latitude differences) received by different slopes on Mars are expected to drive variations in temperature-dependent processes, topographic expressions of such differences should be related to aspect and latitude. The working hypothesis in this study therefore is that temperature-dependent processes should cause detectable, systematic differences in topography (specifically, topographic slope angle) between the north and south walls of Coprates Chasma. The main aim is to determine whether spatial variations in the topography of the trough walls can be shown to be consistent with predicted differentials in the distribution and thermal condition of ground ice within the walls. If such differentials exist, then the following three hypotheses tested in this study will be true: (1) The trough-averaged slope angle of the north wall should be steeper than that of the south, given the colder mean annual surface temperature characteristic of the north wall; (2) the difference in slope angle between the north and south walls should be greatest where expected temperature differentials are greatest, and least where temperature differentials are least (this effectively means that slope angle difference should increase eastward along the trough due to the gradient in latitude); and (3) any along-trough variation or trend in slope angle should be greater along the north wall than the south as the north wall has a more marked trend in predicted mean annual surface temperature (as demonstrated further below) and therefore a greater range of predicted ground ice conditions.

2. Evolution and Stability of Valles Marineris Trough Walls

2.1. Origin of Valles Marineris Troughs

[8] Mechanisms proposed to explain the origin of the equatorial troughs have included processes involving erosion [*McCauley et al.*, 1972; *Tanaka and MacKinnon*, 2000], collapse [*Tanaka and Golombek*, 1988; *Davis and Golombek*, 1990], and tectonism [*Sharp*, 1973; *Blasius et al.*, 1977; *Schultz*, 1991]. A tectonic-structural origin is considered the most reasonable for the large, open troughs (including Coprates Chasma), their formation being related to grabens resulting from a tensional tectonic stress regime associated with the Tharsis Rise. Evidence for such an origin includes boundary faults along trough margins, cliff-type walls, triangular faceted spurs [e.g., *Blasius et al.*, 1977], and down-dropped portions of plateau caprock now residing on the floors of such troughs [e.g., *Lucchitta et al.*, 1992].

[9] *Schultz* [1998] proposed an inclusive, multiple-process origin for the troughs, involving the sequential action of separate processes. The first stage involved the intrusion of dikes [*Mège and Masson*, 1996] radial to Syria Planum during Lower Hesperian time. In a second stage, ancestral basins (closed trough depressions) were formed by subsidence during the Upper Hesperian, followed by the deposition of interior layered deposits within the basins and the formation of chaotic terrain and outflow channels. In the third stage, tectonic grabens were imprinted over the basins as a response to Tharsis-related extension, the configurations of which were again controlled by the dikes [*Schultz*, 1998]. In this third stage, the extension/rifting that formed the Ius Melas-Coprates and Candor-Ophir troughs occurred probably during the Early Amazonian. The troughs have subsequently been widened by erosion [*Schultz*, 1991; *Lucchitta et al.*, 1994].

[10] Coprates Chasma is the longest and deepest of the troughs (Figure 1b). The trough is about 1000 km long, and ranges in depth from 6 km in the eastern section to over 10.5 km in the west, with an average depth of 8 km. The geology is dominated by Noachian wall rock and various trough floor materials of Middle Hesperian age [*Schultz*, 1991] (Figure 1d). Interior layered deposits of Late Hesperian through Middle Amazonian age [*Lucchitta et al.*, 1992] and landslide deposits are not found other than at the

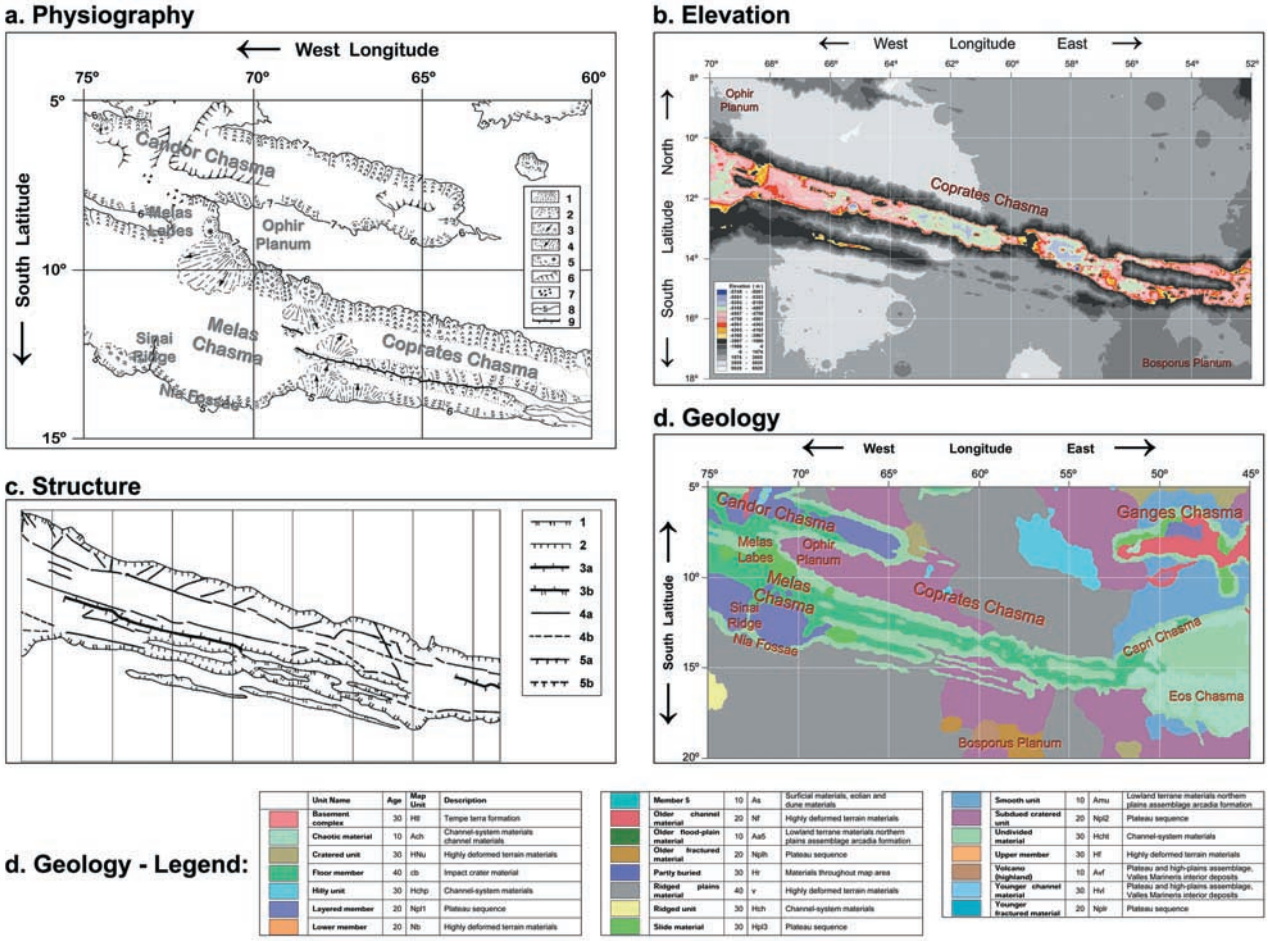

Figure 1. Topography, geology, structure, and physiography of Coprates Chasma. (a) Physiography [from *Peulvast et al.*, 2001]: (1) smooth talus slopes; (2) spurs and gullies slopes; (3) landslide deposits with hummocky material; (4) landslide deposits with hummocky and fan-shaped materials; (5) rotational slumps; (6) aeolian flutes; (7) chaotic terrain; (8) slope gradient; (9) crests. (c) Structure [from *Peulvast et al.*, 2001]: (1) cornice with smooth talus slope; (2) cornice with spurs and gullies; (3a) crest with spurs and gullies on both sides; (3b) crest with spurs and gullies on one side and smooth talus slope on the other side. Structure key: (4a) fault; (4b) conjectured fault; (5a) normal fault; (5b) conjectured normal fault.

western end of the trough, near its confluence with Melas Chasma.

2.2. Geology, Morphology, and Strength of Trough Walls

[11] The walls of the Valles Marineris troughs consist of wallrock topped by a cap rock [e.g., *Lucchitta et al.* 1992, 1994]. MOC images indicate that the vast majority of the wall rock consists of layers 5–50 m thick, and extending at least 5 km below the surface of the surrounding plateau [*McEwen and Malin*, 1998]. The layers show similarities to terrestrial flood basalts in outcrop morphology and may be primarily volcanic in origin, or a mixture of lavas, intrusive magma, and possibly sedimentary rocks [*McEwen and Malin*, 1998; *Malin and Edgett*, 2000; *Williams and Paige*, 2002]. The layers are understood to be of Upper Noachian or Lower Hesperian age (3.1–4.2 b.y.).

[12] Mars Orbiter Laser Altimeter (MOLA) data show that the steepest sections of wallrock achieve slope angles of 30–35°, although some wall slopes achieve gradients of only 12–15° [*Phillips et al.*, 1998; *Schultz*, 2002]. Slope angles decline with decreasing elevation from the local plateau surface [*Phillips et al.*, 1998]. The heights of wall slopes are immense: slope heights measured by *Schultz* [2002] range from 1 to 8 km, and *Peulvast et al.* [2001] report slopes of up to 11 km in height, similar to the maximum trough depth as ascertained by *Lucchitta et al.* [1994].

[13] Under a tectonic-structural origin, the trough walls represent the eroded remains of rift flanks or the footwalls of inward-dipping normal boundary faults [*Schultz*, 1991]. In Coprates Chasma, the faults defining the northern boundary of the trough are more continuous and recently active compared with those defining the southern boundary [*Schultz*, 1991; *Peulvast et al.*, 2001] (Figure 1c). The walls themselves can be divided into two morphological types: those sections that exhibit spur-and-gully morphology, common in straight sections of troughs including along Coprates Chasma; and those sections that are characterized by landslide scars, which are especially frequent in Ius, Ophir, and

Hebes Chasmata [*Lucchitta*, 1978; *Lucchitta et al.*, 1992]. Only three large landslides occur in Coprates Chasma, on the north wall at the west end of the trough [*Lucchitta*, 1979; *Schultz*, 1991]. *Peulvast et al.* [2001] further differentiated these slope types as shown in Figure 1a.

[14] Aspects of the strength and stability of trough wall slopes have been examined by *Schultz* [2002], who assessed the stability of rock slopes in various parts of the chasmata by applying a rock mass strength rating system in conjunction with topographic measurements from MOLA data. Wall rock was shown to be stronger than interior deposits, as indicated by rock mass rating (RMR) values of 50–65 and 30–55 respectively. The values of rock strength are consistent with wall rock slopes being underlain by igneous rock, perhaps jointed basalt [*Schultz*, 2002].

2.3. Trough Wall Erosional Processes and the Possible Role of Volatiles

[15] There has been a substantial amount of backwasting of the trough walls since their initial tectonic-structural formation [*Schultz*, 1991; *Lucchitta et al.*, 1994]. *Lucchitta et al.* [1994] calculated an average erosional widening of the troughs of one-third their original widths on the basis of volumetric calculations of trough topography. *Schultz* [1991] measured a difference between the structural width of the Coprates trough near its western limit (12.3 S, 68 W) of ~60 km and the erosional width in that vicinity of ~100 km. The variable widths of the structural troughs, both between different troughs and within individual troughs, suggest that differential erosional widening has taken place. *Peulvast et al.* [2001] proposed that spatial differences in the volatile content of rock (inferred from data on rampart craters in the surrounding plateaus) may have produced these variations. Other evidence for the role of volatiles in the erosion of the trough walls includes landslides whose morphologies have been interpreted in terms of fluid flow [e.g., *Lucchitta*, 1979, 1987]; channels and tributary canyons suspected to be formed by sapping [*Kochel and Piper*, 1986; *Davis and Golombek*, 1990]; and possible rock glacier features [*Rossi et al.*, 2000; *Whalley and Azizi*, 2003].

[16] Landslides have formed scars of up to 5 km in height in the trough walls [*Lucchitta*, 1979; *McEwen*, 1989]. *Lucchitta* [1979, 1987] concluded on morphologic evidence (e.g., multiple lobes, long runout distances) that the landslides were huge, wet debris flows. Modeling of longitudinal profiles for landslides in Ophir Chasma [*Harrison and Grimm*, 2003] suggests that positive pore water pressures are required to explain the morphology. Deficits between the deposited volumes of landslide material and the calculated volumes of the contributing scars also point to the possible presence of water in the landslides [*Quantin et al.*, 2003]. Water to fluidize the landslides could have been from groundwater, or as ice that was melted during or immediately prior to their occurrence. As an alternative, dry landsliding processes have been suggested by *McEwen* [1989] and *Phillips et al.* [1998]. *McEwen*'s [1989] results concerning landslide morphometry compared closely to data for terrestrial dry-rock avalanches. The Mohr-Coulomb failure criterion analysis of a hypothetical, unfailed trough wall slope by *Phillips et al.* [1998] suggested that groundwater probably did not exist in the upper crust because the trough walls would have exhibited more landsliding than is observed.

[17] *Schultz* [2002] deduced that the landslides in the wallrock were most likely initiated by seisms, because although the wallrock was calculated to be stronger than the interior deposits, only wallrock exhibited landsliding due to the proximity of the walls to trough-bounding faults. Crater data recently reported by *Quantin et al.* [2003] indicate that the landslides have multiple ages, ranging from 1–2 Gyr ago to 100 million years ago. The landslide ages are clustered, which suggests a relationship to distinct, reproducible events such as crater impacts or Marsquakes.

[18] Many parts of the Valles Marineris trough walls not affected by landsliding are characterized by spur-and-gully morphology, including most wall sections of Coprates Chasma (Figure 1a). These walls have spurs and gullies with widths of 15–30 km and slopes of up to 30° [*Peulvast et al.*, 2001]. Some of the spurs are cut by faults, leaving series of triangulated spur facets in some troughs including along the north wall of Coprates. The age and erosional origin of the spur-and-gully morphology remain uncertain. Gullying is indicative of erosion most probably either by water or by interstitial ice [*Lucchitta*, 1978]. *Lucchitta et al.* [1992] likened the morphology of the spur-and-gully walls to that found on scarps in alpine or desert environments on Earth. Alternatively, it is also suggestive of the morphology of the walls of submarine canyons. Therefore the spur-and-gully morphology either relates to a former different climate or is the result of a subaqueous erosional environment [*Lucchitta*, 1999]. The morphology would appear to predate the landslides, as the spurs and gullies are obliterated by them where they occur [*Lucchitta et al.*, 1992; *Peulvast et al.*, 2001], and there is no evidence for their existence on surfaces such as fault scarps and landslide scars.

3. Method

[19] The hypotheses presented in section 1 are tested by (1) measuring the slope angle of Coprates Chasma trough walls as a topographic parameter that should reflect variations in predicted ground ice distribution; (2) establishing the pattern of calculated surface temperature variation along the north and south walls and the differences between them; (3) given the surface temperature pattern, defining the expected distribution of ground ice in the two walls; (4) defining the theoretical effects of temperature and ice on wall strength and slope angle; (5) controlling or otherwise accounting for other potential influences on slope angle variation; and (6) testing the relations between slope angle, surface temperature, and the predicted ground ice distribution.

[20] The data set used for this study was the 1/64 degree gridded MOLA elevation data set. The MOLA elevation data have a ±30 cm vertical accuracy, ~150 m spot size, and ~330 m along-orbital-track spacing. For the purposes of this study, a segment of the data extending 40° West to 85° West by 5° North to 20° South was imported into a GIS environment.

[21] Slope angle was used as a topographic measure that was expected to reflect variations in wall material strength and temperature-related processes. Slope angle has been used by previous authors in studies of geomorphic form and

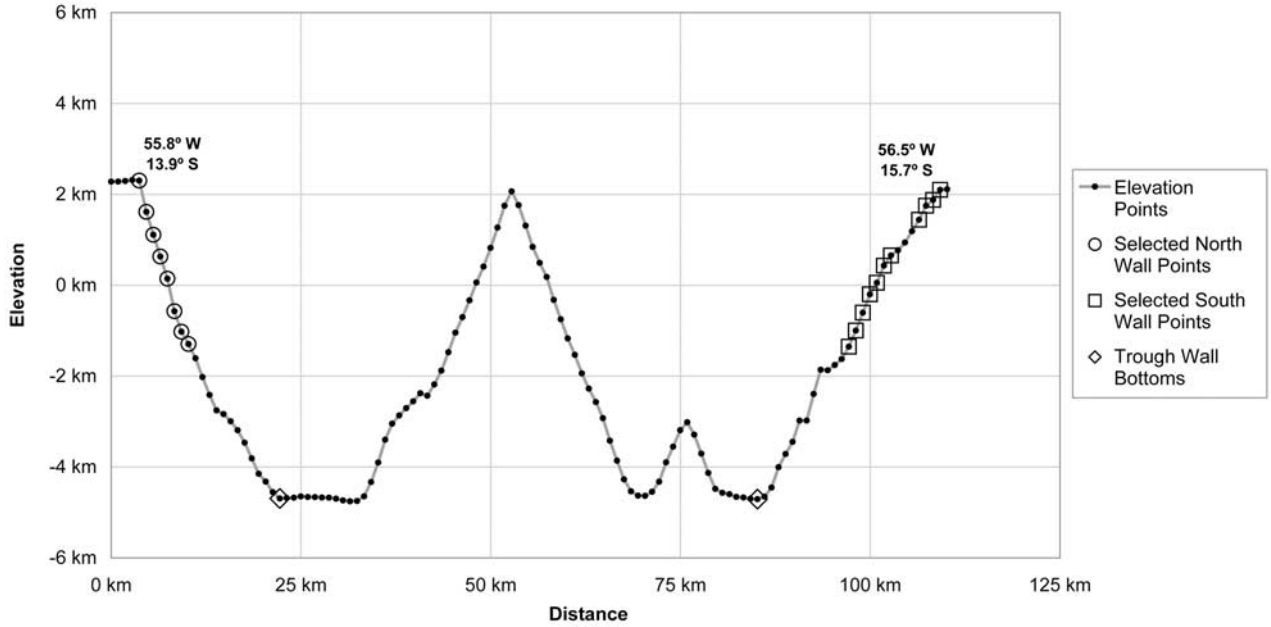

Figure 2. Data points, and points used to measure slope angle for the upper 50% of the walls, for Coprates profile number 200. Profile aspect is 187.2° (north wall)/7.2° (south wall); vertical exaggeration is 6×.

process for features on Earth and Mars [e.g., *Evans*, 1980; *Selby*, 1980; *Davis and Golombek*, 1990; *Schultz*, 2002]. In addition, measurements were also made of trough geometry parameters that included the plateau (trough rim) elevation, trough rim-to-rim width, and trough wall height, all of which were regarded as gross geometric parameters likely to influence variations in slope angle along the north and south walls and differences in slope angle between them. For each wall, correlations were made between slope angle, mean annual surface temperature, location parameters (latitude and longitude), and trough geometry parameters. Ordinary least squares regression was performed to indicate average values of parameters and their trends along the trough, and to establish relations among the various parameters. Comparisons were made for differences in slope angle between the north and south walls using paired-samples t-tests. Differences between the walls in slope angle were correlated with differences in mean annual surface temperature, location, and trough geometry parameters.

4. Profiles Across Coprates Chasma

[22] The purpose of the profiling analysis was to measure various topographic parameters along each wall of the trough. A total of 247 profiles spaced 4 km apart were drawn normal to the trend of the ~1,000-km-long trough, with data points along each profile spaced 926 m apart. The first profile (coprates001) was located at the western-most end of the trough, and the last profile (coprates247) was located at the eastern-most end. The position of the rim on each side of the trough for each profile was defined as the first point that had a slope angle steeper than 5.0° and which was followed by 15 points with an average slope angle steeper than 8.75° (including and starting with the initially selected point) (Figure 2). The position of the trough bottom on each side of the trough for each profile was defined as the bottom-most point of the first 5 points averaging <3.7° found downslope from the rim.

[23] Measurement of wall slope angle was confined to those parts of the profiles comprising the upper 50% of the walls (as measured from trough rim to floor), to discount the possibility of depositional features being included in the analysis (Figure 2). Slope angles along a profile were calculated by using steepest gradient slope angles, with the overall slope angle for a wall at a profile being calculated as the average of the slope angles determined for the relevant points. The steepest gradient slope angles, steepest gradient slope aspects (cosine thereof), and latitudes were used to calculate incidence angles and temperatures for each wall at the location of each profile.

5. Theoretical Predictions

5.1. Calculation of Mean Annual Surface Temperature

[24] Temporal variations in temperature on Mars are generally calculated using the surface energy balance equation:

$$\frac{S_0}{R^2}(1-A_b)\cos i + k\frac{\partial T}{\partial z} + F_a + L\frac{dm}{dt} = \varepsilon\sigma T^4, \qquad (1)$$

where S_0 is the solar constant at 1 AU; R is the mean distance of Mars from the sun; A_b is the bolometric albedo; i is the local incidence angle of sunlight; k is the thermal conductivity of the regolith; F_a is the downward component of atmospheric radiation; L is the latent heat of CO_2 sublimation; m is the mass of CO_2 condensate per unit area; ε is the surface emissivity; and σ is the Stephan-Boltzmann constant [*Kieffer et al.*, 1977; *Clifford*, 1993].

[25] Given the average annual surface temperatures at latitudes equatorward of ~40°, the CO_2 latent heat part of the equation can be ignored for these latitudes. Assuming an

Table 1. Calculated Values of Incidence and Mean Annual Surface Temperature for Three Pairs of Locations Along Coprates Chasma[a]

North/South Wall Latitude, °S	North/South Wall Longitude, °W	Slope Angle, °	North Wall Incidence, °	South Wall Incidence, °	North Wall Mean Annual Surface Temperature, K	South Wall Mean Annual Surface Temperature, K	Difference (North-South), K
10.25/12.00	70 (western end)	15	24.80	2.55	212.1	217.9	−5.8
		20	29.66	7.41	209.6	217.5	−7.8
		25	34.51	12.26	206.7	216.5	−9.8
		30	39.36	17.11	203.5	215.2	−11.7
12.25/14.00	62 (central)	15	26.80	0.55	211.1	218.0	−6.9
		20	31.66	5.41	208.5	217.7	−9.2
		25	36.51	10.26	205.4	217.0	−11.5
		30	41.36	15.11	202.0	215.8	−13.8
14.25/16.00	54 (eastern end)	15	28.80	1.45	210.1	218.0	−7.9
		20	33.66	3.41	207.3	217.9	−10.6
		25	38.51	8.26	204.1	217.3	−13.3
		30	43.36	13.11	200.5	216.3	−15.8

[a]The first row of data is for a location near the western end of the trough; the second row is for a location in the central part of the trough; and the third row is for a location near the eastern end of the trough. Calculated with (assumed) north wall slope aspects of 194° and south wall slope aspects of 14°. Incidence angle is the angle away from vertical. Mean annual surface temperatures were calculated using equation (2); local incidence angles of sunlight were calculated using equation (3).

albedo of A_b = 0.25, a thermal conductivity of k = 2.0 W m^{-1} K^{-1}, and a depth of z = 0, equation (1) can be greatly simplified to provide an equation (equation (2)) for estimating the mean annual surface temperature. Equation (2) is essentially an interpolation of the minimum (154 K) and maximum (218 K) mean annual surface temperatures calculated for Mars by *Clifford* [1993]. Although equation (2) is not a true closed-form solution of equation (1), it provides a satisfactory means by which temperature can be calculated for the purposes of this study.

$$T_{ms} = 64\ \mathrm{K} \cos\ i\ +\ 154\ \mathrm{K}. \quad (2)$$

[26] The local incidence angle, i, depends on latitude, slope angle, and the orientation of the surface (its slope aspect), and is the angle between the incident sunlight and the normal to the planet's surface at that particular latitude. The local incidence angle for a given point on the surface is the absolute value of its latitude, l, minus the north-south component of its slope, β, or

$$i = \mathrm{abs}\ (l - \beta), \quad (3)$$

and where

$$\beta = s \cos a, \quad (4)$$

where s is the steepest gradient slope, and a is the aspect (bearing, orientation) of that steepest gradient slope. Steepest gradient slope is the magnitude of the gradient and slope aspect is the azimuth of the gradient.

5.2. Calculated Temperature and Potential Ice Distribution Differentials

5.2.1. Theoretical Temperature Differences Between the North and South Walls of Coprates Chasma

[27] As an illustration of the magnitude and direction of temperature variations along the walls, and of differences between them, equation (2) was used to calculate T_{ms}, and subsequently to gauge hypothetical ice distribution patterns, for both walls at each of three locations along Coprates Chasma (positioned near the western end of the trough, in its central region, and near the eastern end, respectively) (Table 1). The trough is geographically aligned such that its eastern end lies 4° further south than its western end. The opposing aspects of the south and north walls lead to marked differences in incidence between the two walls, and there are also differences in incidence resulting from slope angle. For a slope angle of 30° (15°), T_{ms} for the south wall increases from west to east by 1.1 K (0.1 K), but the temperature of the north wall decreases by 3 K (2 K) along the same direction (Table 1). The effect of aspect is seen by the differentials for each location, with the T_{ms} of the south wall being warmer than the north by 11.7 K (5.8 K), 13.8 K (6.9 K), and 15.8 K (7.9 K) at the western, central, and eastern sections of the trough respectively. As an illustration of the variation in mean annual surface temperature across the trough, temperature variation was calculated using actual data from profile 200 using equation (5), as shown in Figure 3.

5.2.2. Depth to the Base of the Cryosphere in Coprates Chasma

[28] The depth to the base of the cryosphere (z) can be estimated using the steady state one-dimensional heat conduction equation:

$$z = K \frac{T_{mp} - T_{ms}}{Q_g}, \quad (5)$$

where K is the thermal conductivity of the Martian crust, T_{mp} is the melting point of ground ice, T_{ms} is the mean annual surface temperature, and Q_g is the value of the geothermal heat flux. The values used here are those reviewed and used by *Clifford* [1993] of Q_g = 30 mW m^{-2}, K = 2.0 W m^{-1} K^{-1}, and T_{mp} = 252 K.

[29] Substituting the temperature data of Table 1 (for a wall slope angle of 25°) into equation (5) shows that for the eastern end of the trough the calculated depth to the base of the cryosphere underneath the south wall is ~2.3 km and under the north wall is ~3.2 km; the comparable values for the western end of the trough are ~2.4 and ~3.0 km respectively. All other factors being equal, there is therefore a substantial predicted difference in the depth to the cryosphere between the south and north walls of Coprates Chasma, with the difference being greater at the eastern end of the trough. *McGovern et al.* [2002] revised Q_g downward to around 20 mW m^{-2}; use of such a value in

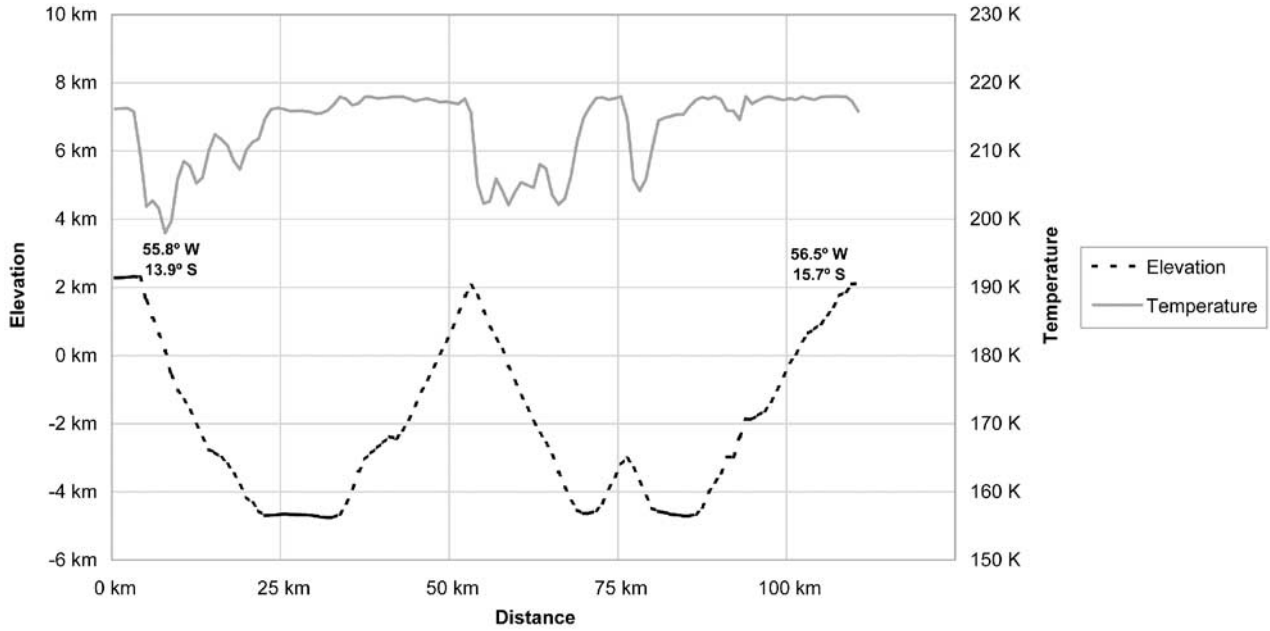

Figure 3. Calculated temperature variation along Coprates profile number 200. Vertical exaggeration of elevation profile is 5×.

these calculations would increase the estimated depths to the base of the cryosphere, and the N-S differentials, by 50%.

[30] As an illustration of the variation in the depth to the base of the cryosphere across the trough, the depth variation (Figure 4) was calculated using actual data from profile 200 using equation (5) and the variation in surface temperature and slope angle as displayed in Figure 3. With nominal parameters (Q_g = 30 mW m^{-2}, K = 2.0 W m^{-1} K^{-1}, and T_{mp} = 252 K [*Clifford*, 1993]), this calculation yields a depth to the base of the cryosphere of ~2.3 km under the south wall of the trough and ~3.6 km under the north wall in the vicinity of profile 200.

5.2.3. Depth to the Ice Table in Coprates Chasma

[31] The ice table represents the depth below which ground ice theoretically exists in the cryosphere, with the depth being a function of mean surface temperature and the thermal conductivity of the crust. Thermal models indicate the equatorial region has been desiccated to leave the ice

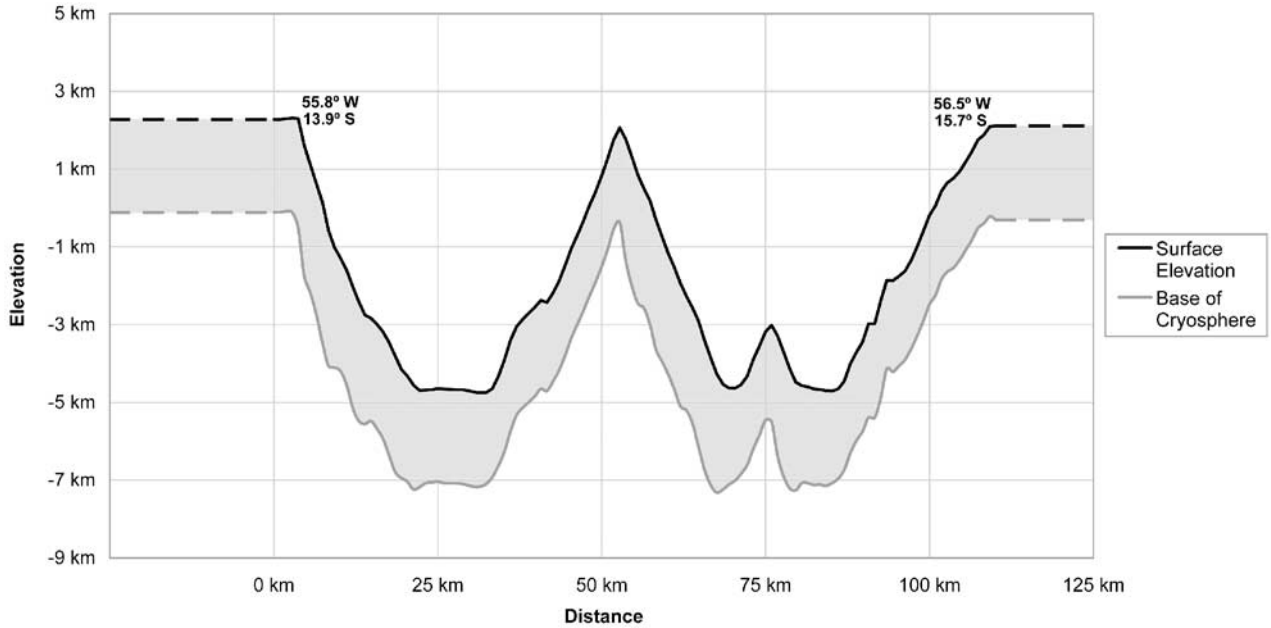

Figure 4. Coprates Chasma profile number 200 with hypothetical cryosphere. Depth to cryosphere calculated using equation (5); nominal values cited for Mars are Q_g = 30 mW m^{-2}, K = 2.0 W m^{-1} K^{-1}, and T_{mp} = 252 K [*Clifford*, 1993]; T_{ms} was calculated using equation (2); vertical exaggeration is 6×.

table a postulated ~100–300 m below the surface [*Clifford and Hillel*, 1983; *Fanale et al.*, 1986; *Mellon et al.*, 1997]. Whether or not the ice table is regarded as being in a steady state condition, it is likely to be shallower underneath the north wall of Coprates Chasma, given that the ice table depth is dependent upon mean annual surface temperature, and given the calculated differential in surface temperature between the north and south walls.

[32] *Mellon et al.* [1997] considered the possibility of a steady state ice table in the equatorial regions, and for a thermal conductivity of 1.0 W m^{-1} K^{-1} (representing "dense rock") the ice table is calculated to have a depth of ~300 m for a T_{ms} of 217 K (equating to the south wall), and a depth of ~200 m for a T_{ms} of 200 K (equating to the north wall). The corresponding temperatures at the ice table for the relevant surface temperature conditions are 225 K and 205 K for the south and north walls respectively (data from *Mellon et al.* [1997]).

5.3. Consequences of Temperature Differences for Ground Ice Distribution and for Spatial Variation in the Strength and Morphology of Coprates Chasma Walls

[33] As demonstrated, insolation differences between the south and north walls of Coprates Chasma are predicted to generate differences in T_{ms} between the two walls. The differences in T_{ms} are in turn expected to cause differences in subsurface temperatures (for equal depths) in the material comprising the trough walls, and also to influence the depths to the ice table and to the base of the cryosphere within the trough walls. Given that the existence of near-surface liquid water is precluded by current (and past) atmospheric temperature and pressure conditions [e.g., *Fanale*, 1976], the trough wall constituent materials within the part of the cryosphere below the ice table will either contain ground ice or be dry. Whether or not the cryosphere contains ground ice will determine the strength and susceptibility to erosion of the trough walls, and therefore the morphology of the walls. Thus hypothesized patterns of wall morphology are able to be established on the basis of the predicted distribution of ground ice, as outlined below.

5.4. Development of Hypotheses

[34] If ground ice were present within the constituent materials of the trough walls, it would affect the strength (erodability) of the walls. Any ice-laden material comprising the north wall would be colder than in the south wall and would therefore be more stable in terms of ice-related deformation than would the south wall. In approximate terms, given this temperature differential, the strain rate of ice would be 20 times lower in the northern wall and would constitute a strength difference between the walls. Because of the differential between the walls in the depth to the cryosphere (calculated to be 600–1400 m deeper below the north wall, dependent on location along the trough), there would also be a greater thickness of ice-rich material underlying the north wall, and which for equivalent depths would be colder than the south wall.

[35] The mechanical effect of sublimation of interstitial volatiles is to reduce the strength of the material by removing the component of total material strength provided by ice, so that the desiccated material is weaker and more easily eroded than the ice-saturated material [e.g., *Moore et al.*, 1996; *Peulvast et al.*, 2001]. In Coprates Chasma, if the hypothesized asymmetries in ground ice distribution are correct, colder slopes should exhibit steeper slope angles than warmer slopes, because the rate of sublimation and therefore weakening of desiccated material is slower, the depth to the ice table is shallower, and the ice-laden material at and below the ice table is colder and stronger. Given that the ice table in the north wall is hypothesized to have colder, stronger ice than the south wall, the slope would maintain a steeper topographic slope angle during erosion.

[36] Asymmetries in surface temperature and ice distribution between the north and south walls of the trough would therefore produce predictable differences in slope material strength and slope angle. Specifically, if ground ice were differentially distributed according to the spatial pattern of mean annual surface temperature as described, the following hypotheses would be found to be true:

[37] H1. The trough-averaged slope angle of the north wall should be steeper than that of the south wall.

[38] H2. The difference in slope angle between the north and south walls should be greatest where temperature differentials are greatest and least where temperature differentials are least. Essentially, this means that slope angle difference should increase eastward along the trough.

[39] H3. Any along-trough trend in slope angle should be greater along the north wall than the south as the north wall has a more marked trend in predicted mean annual surface temperature and consequently a greater range of ground ice conditions.

[40] If ground ice were absent from the constituent materials of the trough walls, that is, the materials were dry, the effect of insolation and temperature asymmetries would be different from the ice-present scenario. Because of the absence of an asymmetric distribution of ice and a differential in its thermal condition, there would be no resultant strength differential (attributable to ground ice) between the material comprising the north and south walls respectively. Therefore, if no ground ice were contained within the walls, hypotheses H1–H3 presented above would be rejected.

6. Empirical Results

6.1. Slope Angle Variations and Differences

[41] The slope angle of the walls as determined from the profiles ranges from 14 to 29°. The average slope angle of the north wall is 22.4 ± 0.3° and of the south wall is 21.1 ± 0.4° (Table 2). The slope angle of both the north and south walls increases, on average, from west to east along the trough (Figure 5). However, there is some scatter in the data (standard deviations: north wall 2.4°; south wall 2.9°). The average difference in slope angle between the two walls is 1.3° ± 0.5°, with the north wall being steeper than the south. The difference in slope angle between the walls is, on average, the same at all locations along the trough, as shown in both Figure 5 and Figure 6. A greater number of wall slope sections are steeper on the north wall of the trough (157) than on the south (90).

6.2. Mean Annual Surface Temperature Variations and Differences

[42] Calculated values of T_{ms} for the south wall are higher than those for the north wall, with a difference of

Table 2. Coprates Chasma North and South Wall Data

	Mean (±95% CI)	North Minus South Difference (±95% CI)
Incidence angle	N: 32.4 ± 0.4° S: 6.7 ± 0.3°	25.7 ± 0.6°
Temperature	N: 207.7 ± 0.3 K S: 217.4 ± 0.0 K	−9.7 ± 0.3 K
Slope	N: 22.4 ± 0.3° S: 21.1 ± 0.4°	1.3 ± 0.5°
Aspect	N: 192 ± 3° S: 11° ± 3°	−179 ± 4°
Wall height	N: 8,095 ± 164 m S: 7,299 ± 178 m	796 ± 149 m
Rim elevation	N: 3,408 ± 153 m S: 2,656 ± 160 m	752 ± 140 m
Bottom elevation	N: −4,686 ± 48 m S: −4,643 ± 59 m	−43 ± 64 m

∼7.5 K at the western end of the trough and ∼11.5 K at the eastern end (Figure 7). Calculated T_{ms} along the north wall decreases significantly along the trough from west to east, although the data show considerable scatter. In contrast, there is little variation and negligible trend in mean surface temperature along the trough for the south wall. The calculated temperature difference widens along the trough, due to the decline in temperatures along the north wall from 210 K to 206 K. The average calculated T_{ms} for the north wall is 207.7 K and for the south is 217.4 K (Table 2), with the average difference in temperature being 9.7 K.

6.3. Relationships Between Slope Angle and Slope Angle Difference and Other Variables

6.3.1. Slope Angle

[43] For the north wall, slope angle has small but significant correlations with longitude and latitude (Figure 5 and Table 3). The slope angle of the south wall has a significant negative correlation with trough rim-to-rim width and with trough bottom elevation, but is not significantly correlated with either latitude or longitude.

6.3.2. Slope Angle Difference

[44] The north-south wall difference in slope angle has no significant correlation with wall height or with the difference in either wall height or rim elevation (Table 4). However, it has a significant positive correlation with trough width, which is due mainly to the decrease in slope angle of the south wall with respect to trough width.

6.4. Hypothesis Testing and Interpretation

6.4.1. Hypothesis Testing

[45] On the basis of the empirical results presented, the outcomes of testing the hypotheses are as follows:

[46] H1 is accepted. The trough-averaged slope angle of the north wall is 1.3° ± 0.5° steeper than that of the south wall.

[47] H2 is rejected. The average difference in slope angle between the north and south walls is constant along the trough, despite a difference in average T_{ms} of ∼7.5 K at the western end of the trough and ∼11.5 K at the eastern end.

[48] H3 is rejected. The along-trough trend in slope angle is the same (a 1.5° increase from west to east) for both walls, despite T_{ms} for the north wall decreasing by 4 K and T_{ms} for the south wall being essentially constant.

6.4.2. Interpretation: Influence of Surface Temperature on Slope Angle

[49] Although the north wall is on average 1.3° steeper, and on average 9.7 K colder, than the south wall of the trough (Table 2), the difference in slope angle between the walls does not systematically increase from west to east along the trough as predicted; the slope angle differential is therefore unlikely to be related in a simple manner to differentials in T_{ms}. In addition, the average slope angle at the eastern end of the south wall is the same as the average slope angle at the western end of the north wall, despite a calculated T_{ms} difference of 7–8 K. Furthermore, the increase in average slope along the trough for the south

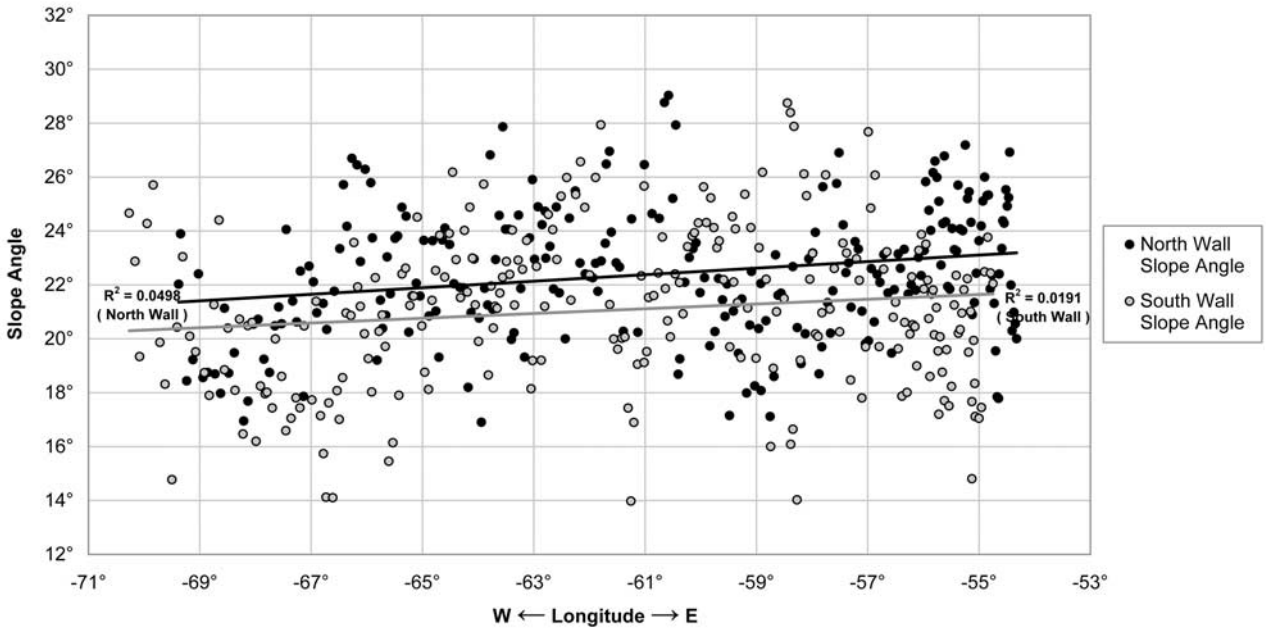

Figure 5. Variation in slope angle with longitude for north and south walls.

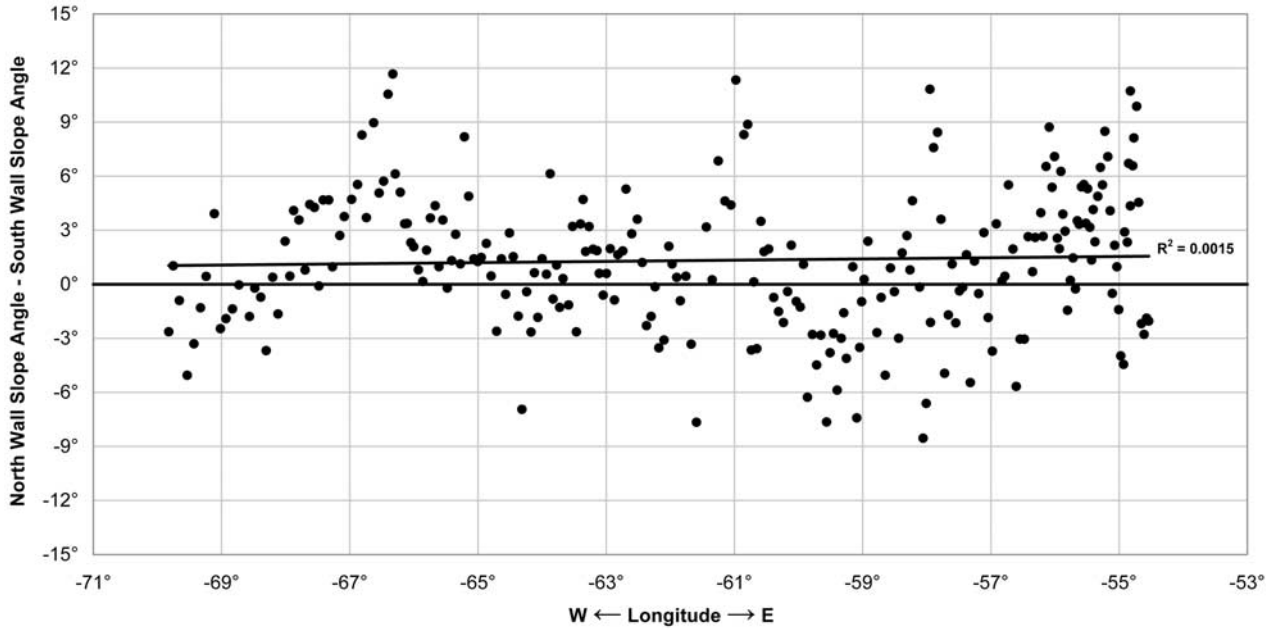

Figure 6. Variation in slope angle difference with longitude.

wall is the same as for the north wall, despite the essentially constant surface temperature along the south wall. These observations suggest that variations in wall slope angle have little relation to surface temperature variations and hence to hypothesized ground ice distribution patterns.

7. Discussion

7.1. Role of Volatiles in the Strength and Erosion of Trough Walls

[50] Although the presence of ice and its sublimation have been previously referred to as possible causes of variations in wallrock strength and erodability in Valles Marineris [e.g., *Peulvast et al.*, 2001; *Mège and Gatineau*, 2003], the evidence for it to date has been largely circumstantial. *Peulvast et al.* [2001] used ejecta mobility data from rampart craters on the plateaus in the vicinity of Valles Marineris to make inferences about material rheology, which they argued reflected variations in host rock volatile (ice) content and therefore in the strength (erodability) of trough wall rock. They found a loose correlation between high values of host rock ice content and the areas of greatest trough widening (central troughs), and attributed this to the former presence of ground ice where sublimation of the ice

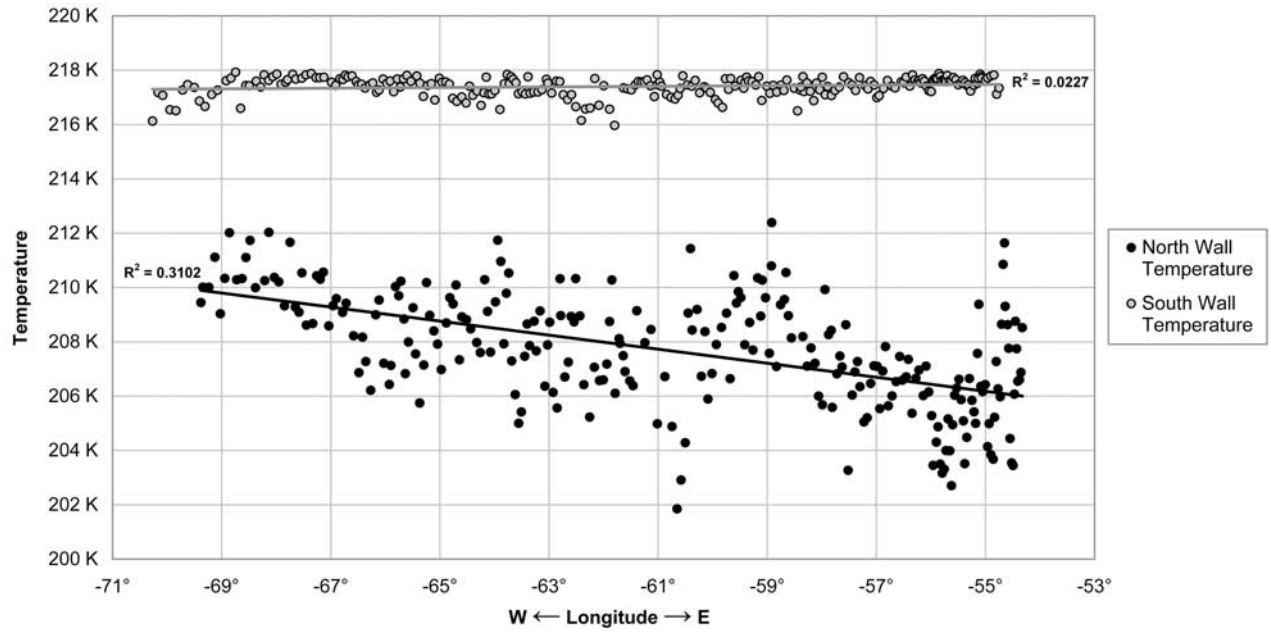

Figure 7. Mean surface temperature variation with longitude for Coprates Chasma. Spearman rank correlation for north wall data is −0.56 ($p < 0.000$) and for south wall data is 0.12 ($p = 0.06$).

Table 3. Spearman Rank Correlations of Slope Angle With Location and Trough Geometry Parameters for North and South Walls[a]

	Latitude	Longitude	Width at Rims	Width at Bottoms	Wall Height	Rim Elevation	Bottom Elevation
			North Wall Slope Angle				
Correlation coefficient	−0.224[b]	0.222[b]	−0.052	−0.091	−0.155[c,d]	−0.065	0.101
Sig. (2-tailed)	0.000	0.000	0.415	0.155	0.015	0.309	0.113
			South Wall Slope Angle				
Correlation coefficient	−0.118	0.110	−0.368[b]	−0.108	0.046	−0.017	−0.332[b]
Sig. (2-tailed)	0.063	0.083	0.000	0.092	0.476	0.786	0.000

[a]N = 247 for all correlations.
[b]Correlation is significant at the 0.01 level (2-tailed).
[c]Correlation is significant at the 0.05 level (2-tailed).
[d]Correlation can be ignored as wall height data are bimodal.

matrix had reduced the strength of materials into which the wall surfaces were eroding. Trough walls with lesser amounts of wall retreat (eastern and western troughs) were interpreted as having lower proportions of cryospheric volatiles due, perhaps, to being less porous. However, the spatial patterns of material property values produced were in fact somewhat loosely constrained, and based on the assumption that the properties of the rock already eroded by the widening troughs were similar to those of the rock constituting the surrounding plateaus.

[51] In contrast to the findings of *Peulvast et al.* [2001], the results of this study are at variance with the idea that wall strength and rates/amounts of erosion have been controlled by differentials in ice distribution within trough wall-forming materials. The observed pattern of wall slope angle variation within the trough is not consistent with the hypothesized distribution and condition of ground ice within the walls, on the basis of three points of evidence. First, the difference in slope angle between the north and south walls, contrary to predictions based on asymmetrical patterns of temperature and of predicted ground ice distribution, does not increase eastward along the trough. Second, the sections of wall at the east end of the south wall and at the west end of the north wall have the same average slope angle but temperatures that differ by some 7–8 K. Third, the increase in average slope angle along the trough for the south wall (about 1.5° from west to east) is the same as for the north wall, but with no change in surface temperature. The major inference drawn from the results is that ice has been absent from the slope-forming materials underlying the walls of Coprates Chasma for geologically significant timescales, corresponding to the time since the spur-and-gully morphology was formed (early Middle Amazonian). An additional test of the possible influence of volatiles on wall erodability is that the westward increase in host rock volatile concentration along Coprates Chasma as proposed by *Peulvast et al.* [2001] would be expected to produce a westward widening of the trough. However, the topographic data used in the current study show that the trough measures 100–125 km in both the eastern and western sections and pinches to 70–105 km in the central section (Figure 1b).

7.2. Constraints on the Formation of Spur-and-Gully Morphology and on Landsliding

[52] The dominant type of erosional morphology of the walls of Coprates Chasma is spur-and-gully morphology, with a few landslides being confined to the western end of the trough. The age of the spur-and-gully erosion is not certain [e.g., *Lucchitta*, 1999], although the morphology is destroyed by landslides where they occur (in both western Coprates Chasma, and more extensively in other troughs), and the erosional style does not seem to have developed on the landslide headscarps nor on young fault scarps [*Lucchitta*, 1979; *Lucchitta et al.*, 1992]. The landslides must therefore post-date the formation of the spur-and-gully erosion. Recent dating of landslides by *Quantin et al.* [2003] in Valles Marineris indicates that the landslides have occurred in ''batches'' with ages ranging from 1–2 Gyr to 100 million years. This result would seem to discount the possibility that spurs and gullies could be actively forming on landslide headscarps as it would have started to appear after 1–2 Gyr of erosion on the older scars. A maximum age for the onset of erosion of the spur-and-gully morphology is Early Amazonian, given that its development post-dates the formation of grabens on Ophir Planum [*Blasius et al.*, 1977; *Schultz*, 1991, 1998]. In addition, the timing of the erosion would also appear to be restricted by its onlap onto the morphology of interior layered deposits aged Late Hesperian through to Middle Amazonian [*Schultz*, 1991; *Komatsu et al.*, 1993]. The spur-and-gully topography is therefore a relict topography dating back to around the early Middle Amazonian.

Table 4. Correlations of Slope Angle Difference With Location and Trough Wall Geometry Parameters[a]

	North Wall and South Wall Data						
	Latitude	Longitude	Width at Rims	Width at Bottoms	Rim Elevation Difference	Bottom Elevation Difference	Wall Height Difference
Slope angle difference							
Correlation coefficient	−0.027	0.053	0.251[b]	0.001	0.085	0.052	0.053
Sig. (2-tailed)	0.674	0.409	0.000	0.990	0.185	0.412	0.403

[a]N = 247 for all correlations.
[b]Correlation is significant at the 0.01 level (2-tailed).

[53] The spur-and-gully morphology could conceivably have been produced either by dry mass wasting characteristic of a cold climate [e.g., *Blasius et al.*, 1977; *Sullivan*, 1992], or by running water, or by subaqueous processes when the trough was flooded or filled by a lake [e.g., *Lucchitta et al.*, 1994]. *Sullivan* [1992] suggested that the spur-and-gully morphology is a result of periodic removal of weathered debris by avalanche chute movements of depths ranging up to 150 m. The cycle starts with the weathering and weakening of trough wall surface materials until a critical thickness of material is reached and removed under the stress of its own weight by mass movement. The weakening of layers to depths of up to 150 m was postulated to be due to the sublimation of ice, with the bases of rock avalanches being activated at the ice table which would be expected to provide a strength discontinuity. The results of this study do not support the dry mass wasting origin for the spur-and-gully morphology with erosion rates controlled by the sublimation of ice. There is no topographic signature consistent with the expected three-dimensional distribution of ground ice along the trough, or with its differential distribution across the two walls, that supports such an origin. Such an origin, if ice were involved, should have given rise to topographic asymmetries and patterns consistent with differentials in the distribution and strength of ice across the two walls. If the role of ground ice in the formation of the spur-and-gully topography can thus be ruled out, this constrains the origin of the morphology to the action of liquid water, either by overland/subsurface flow or by submarine processes [*Lucchitta*, 1978; *Lucchitta et al.*, 1994]. In addition, given the inferred absence of ground ice within the trough walls during the period when landslides were destroying the spur-and-gully morphology in some wall sections, it seems evident that the initiation and mobilization of these mass movements did not involve ice, at least in the walls of Coprates Chasma. Existing explanations of landslide initiation that involve the melting of ice therefore need to be re-evaluated.

7.3. Alternative Explanations of Trough Wall Slope Variation

[54] Several processes or mechanisms not involved with volatiles could conceivably have caused slope angle variation (including opposing wall asymmetry) in trough walls. These include gross variations/differences in trough geometry (e.g., trough depth), structural/tectonic mechanisms [*Schultz*, 1991; *Peulvast et al.*, 2001; *Mège and Gatineau*, 2003], and rock mass strength mechanical stability differences [*Schultz*, 2002; *Mège and Gatineau*, 2003]. Correlations of slope angle and slope angle difference with trough geometry factors such as rim elevation and wall height as determined in this study are fairly weak or insignificant, even though these parameters exhibit variation along the trough and show differences between opposing walls. These results suggest that trough geometric factors have little bearing on slope angle variations along the trough walls or on slope angle differences between the two trough walls.

[55] Structural and tectonic processes could potentially impart variations in erosion and topography along each wall, and produce differentials in slope angle between the walls. The slope angle asymmetry measured, for example, could be produced by an asymmetric graben structure. Coprates Chasma exhibits a strong graben-like form, its tectonic origin reflected by inward-dipping normal boundary faults and interior fault scarps [*Schultz*, 1991]. *Schultz*'s [1991] study of the structural development of the trough led him to conclude that the cross-sectional geometry of the trough may be characterized by a subtle, down-to-the-north half-graben structure, with the master fault running along the northern margin of the trough. However, he recognized that better data were needed to detect topographic trends (such as a sloping trough floor, a good indicator of the presence of structural asymmetry) to verify the asymmetric graben hypothesis. Wall bottom elevations measured in this study and which mark the level of the trough floor at the base of each wall show no statistical difference between the north and south walls as judged using a paired t-test (Table 2). On this evidence, it is concluded that the average across-trough slope gradient of the trough floor is negligible, and that Coprates Chasma is most likely a symmetric graben. The measured trough wall slope angle asymmetry (north wall on average steeper) is therefore unlikely to be a result of asymmetric graben geometry.

[56] A final, and favored, possibility to explain the variation in slope angle and slope angle difference along the trough concerns local and regional contrasts in the rock mass strength of wallrock [*Schultz*, 2002; *Mège and Gatineau*, 2003], bearing in mind that the results presented here preclude differences in wall strength resulting from variations in ice content or in the variable desiccation of wall material [cf. *Peulvast et al.*, 2001; *Mège and Gatineau*, 2003]. The topographic slopes measured exhibit an angle-height pattern that cuts across lines of equal rock mass rating (strength) (Figure 8), interpreted as meaning that the wallrock constituting the slopes exhibits spatial variation in its resistance to erosion. The inferred strength of the wallrock is inferred to be an RMR of 50–75, characteristic of a reasonably coherent but well-jointed rock mass [*Schultz*, 2002]. Any variations in the orientation and dip of the layering and joints of the wallrock, or in joint continuity and density, would affect the rock mass strength of the rock [*Selby*, 1980; *Bieniawski*, 1989; *Schultz*, 2002; *Mège and Gatineau*, 2003], and could explain some of the variation in slope angle along each trough wall.

8. Conclusion

[57] This study has used a novel approach to investigate aspects of the evolution of the trough walls in Coprates Chasma, with particular reference to the possible role of ice and to the formation of spur-and-gully morphology. The investigation set out to discover whether the pattern of slope angle variation of the walls is consistent with the hypothesized presence of ground ice within the walls. Calculated mean annual surface temperature variations along each wall, and temperature differences between the two walls, were used to define the predicted three-dimensional distribution, thermal condition, and strength of ground ice. The observed wall slope angle variation is not consistent with the predicted distribution and condition of ground ice. It is inferred that the erosional morphology of the trough walls is not a function of ice-related processes, and that ground ice has been absent for most or all of the time since the spur-and-gully topography formed (around the early Middle Amazonian).

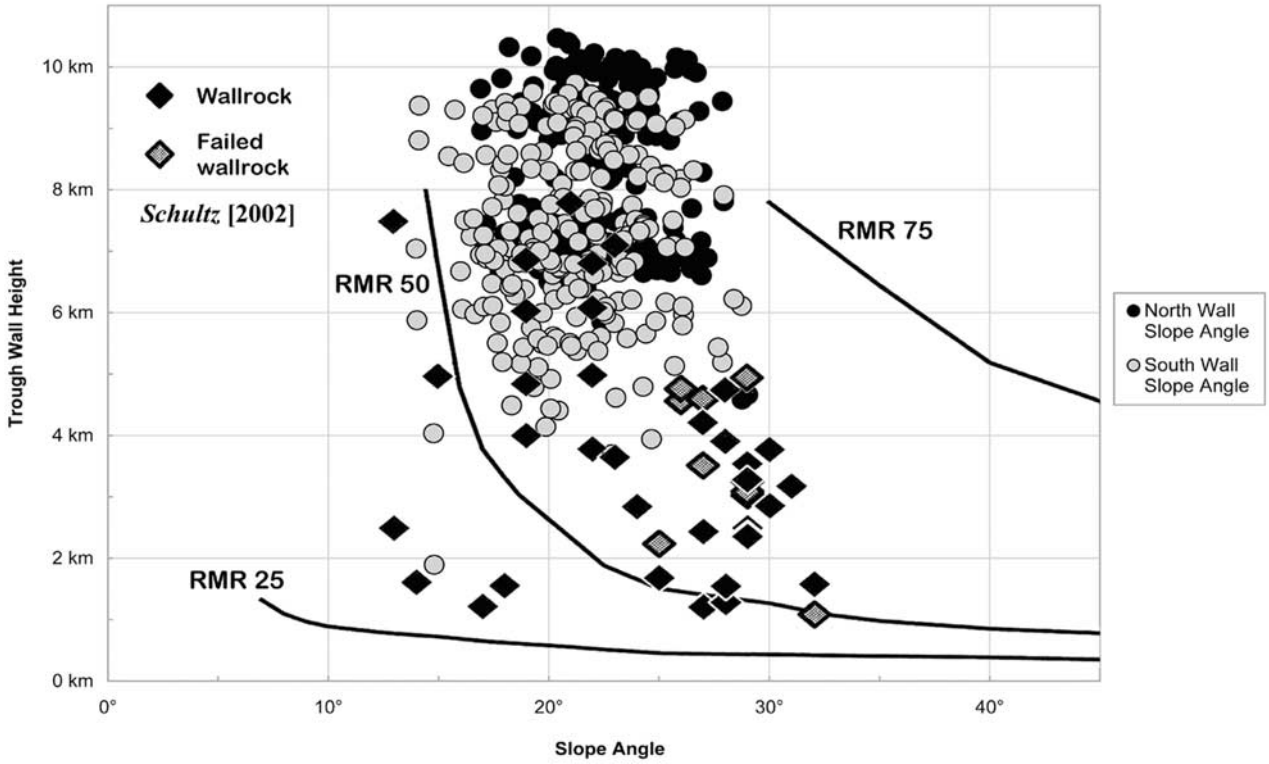

Figure 8. Coprates Chasma trough wall slope angle and height data superimposed on the results of *Schultz* [2002]. RMR, Rock Mass Rating.

[58] Given the apparent longevity of the spur-and-gully morphology, and because the topographic patterns presented indicate the absence of ground ice, it is likely the spurs and gullies were formed by the action of liquid water (either subaerial or submarine) and not by dry mast-wasting above an ice-rich crust. Landslides, where they occur in the spur-and-gully morphology in Coprates Chasma, have by implication neither been initiated by ice-related processes nor mobilized by ground ice. These findings demand a reconsideration of the role/non-role of volatiles in influencing both the erosional susceptibility of the trough walls and the dynamics of the contributing slope-forming processes. The evolution of the spur-and-gully morphology is still not well understood and the morphology remains under-studied (compared with landslide wall sections) given that it is the predominant wallrock form in Valles Marineris. Insights into its form and evolution could be gained from a detailed morphometric analysis using MOLA topography.

[59] **Acknowledgments.** I gratefully acknowledge funding for this work from the Research Council of Norway through doctoral fellowship number NFR 128197/410 (later 128197/410/bg). I thank the Lunar and Planetary Institute for their hospitality and Rice University for additional financial support. Eystein Husebye at the University of Bergen is acknowledged for facilitating the completion of this project. I thank Steve Clifford, Dale Sawyer, and two anonymous reviewers for providing critical and constructive comments on earlier versions.

References

Andersland, O. B., and B. Ladanyi (1994), *An Introduction to Frozen Ground Engineering*, Chapman and Hall, London, England.

Bieniawski, Z. T. (1989), *Engineering Rock Mass Classifications*, John Wiley, New York.

Blasius, K. R., J. A. Cutts, J. E. Guest, and H. Masursky (1977), Geology of the Valles Marineris: First analysis of imaging from the Viking 1 Orbiter primary mission, *J. Geophys. Res.*, *82*(B28), 4067–4092.

Bourbonnais, J., and B. Ladanyi (1985a), The mechanical behavior of frozen sand down to cryogenic temperatures, in *Proceedings of the 4th International Symposium on Ground Freezing, Sapporo, Japan*, vol. 1, pp. 235–244, A. A. Balkema, Brookfield, Vt.

Bourbonnais, J., and B. Ladanyi (1985b), The mechanical behavior of a frozen clay down to cryogenic temperatures, in *Proceedings of the 4th International Symposium on Ground Freezing, Sapporo, Japan*, vol. 2, pp. 237–244, A. A. Balkema, Brookfield, Vt.

Boynton, W. V., et al. (2002), Distribution of hydrogen in the near surface of Mars: Evidence for subsurface ice deposits, *Science*, *297*, 81–85.

Carr, M. H. (1981), *The Surface of Mars*, Yale Univ. Press, New Haven, Conn.

Clifford, S. M. (1993), A model for the hydrologic and climatic behavior of water on Mars, *J. Geophys. Res.*, *98*(E6), 10,973–11,016.

Clifford, S. M. (2003), The limits of theoretical modeling and geomorphic interpretation in assessing the present distribution of subsurface H_2O on Mars, *Proc. Lunar Planet. Sci. Conf. 34th*, abstract 2118.

Clifford, S. M., and D. Hillel (1983), The stability of ground ice in the equatorial regions of Mars, *J. Geophys. Res.*, *88*(B3), 2456–2474.

Costard, F. M. (1989), The spatial distribution of volatiles in the Martian hydrolithosphere, *Earth Moon Planets*, *45*(6), 265–290.

Davis, P. A., and M. P. Golombek (1990), Discontinuities in the shallow Martian crust at Lunae, Syria, and Sinai Plana, *J. Geophys. Res.*, *95*(B8), 14,231–14,248.

Durham, W. B., S. H. Kirby, and L. A. Stern (1992), Effects of dispersed particulates on the rheology of water ice at planetary conditions, *J. Geophys. Res.*, *97*(E12), 20,883–20,897.

Evans, I. S. (1980), An integrated system of terrain analysis and slope mapping, *Zeitschr. Geomorphol.*, *36*, 274–295.

Fanale, F. P. (1976), Martian volatiles: Their degassing history and geochemical fate, *Icarus*, *28*, 179–202.

Fanale, F. P., J. R. Salvail, A. P. Zent, and S. E. Postawko (1986), Global distribution and migration of subsurface ice on Mars, *Icarus*, *67*, 1–18.

Farmer, C. B., and P. E. Doms (1979), Global and seasonal water vapor on Mars and implications for permafrost, *J. Geophys. Res.*, *84*(B6), 2881–2888.

Feldman, W. C., et al. (2002), Global distribution of neutrons from Mars: Results from Mars Odyssey, *Science*, *297*, 75–78.
Gooding, J. L., R. E. Arvidson, and M. Y. Zolotov (1992), Physical and chemical weathering, in *Mars*, edited by H. H. Kieffer et al., pp. 626–651, Univ. of Ariz. Press, Tucson.
Harrison, K. H., and R. E. Grimm (2003), Rheological constraints on Martian landslides, *Icarus*, *163*, 347–362.
Kieffer, H. H., T. Z. Martin, A. R. Peterfreund, B. M. Jakosky, E. D. Miner, and F. D. Palluconi (1977), Thermal and albedo mapping of Mars during the Viking primary mission, *J. Geophys. Res.*, *82*(28), 4249–4292.
Kochel, R. C., and J. F. Piper (1986), Morphology of large valleys on Hawaii: Evidence for groundwater sapping and comparisons with Martian valleys, *Proc. Lunar. Planet. Sci. Conf. 17th*, Part 1, *J. Geophys. Res.*, *91*, suppl., E175–E192.
Komatsu, G., P. E. Geissler, R. G. Strom, and R. B. Singer (1993), Stratigraphy and erosional landforms of layered deposits in Valles Marineris, Mars, *J. Geophys. Res.*, *98*(E6), 1105–1121.
Kuzmin, R. O., N. N. Bobina, E. V. Zabalueva, and V. P. Shashkina (1988a), Structural inhomogeneities of the Martian cryolithosphere, *Sol. Syst. Res.*, *22*, 195–212.
Kuzmin, R. O., N. N. Bobina, E. V. Zabalueva, and V. P. Shashkina (1988b), Inhomogeneities in the upper levels of the Martian cryolithosphere (abstract), *Proc. Lunar Planet. Sci. Conf. 19th*, 655–656.
Leighton, R. B., and B. C. Murray (1966), Behavior of carbon dioxide and other volatiles on Mars, *Science*, *153*, 136–144.
Lucchitta, B. K. (1978), Morphology of chasma walls, *J. Res. U.S. Geol. Surv.*, *6*, 651–662.
Lucchitta, B. K. (1979), Landslides in Valles Marineris, Mars, *J. Geophys. Res.*, *84*(B14), 8097–8113.
Lucchitta, B. K. (1987), Valles Marineris, Mars: Wet debris flows and ground ice, *Icarus*, *72*, 411–429.
Lucchitta, B. K. (1999), Mysteries of Valles Marineris: What can we learn from future exploration?, *Proc. Lunar Planet. Sci. Conf. 30th*, abstract 1297.
Lucchitta, B. K., A. S. McEwen, G. D. Clow, P. E. Geissler, R. B. Singer, R. A. Schultz, and S. W. Squyres (1992), The canyon system on Mars, in *Mars*, edited by H. H. Kieffer et al., pp. 453–492, Univ. of Ariz. Press, Tucson.
Lucchitta, B. K., N. K. Isbell, and A. Howington-Kraus (1994), Topography of Valles Marineris: Implications for erosional and structural history, *J. Geophys. Res.*, *99*(E2), 3783–3798.
Malin, M. C., and K. S. Edgett (2000), Sedimentary rocks of early Mars, *Science*, *290*, 1927–1937.
McCauley, J. F. (1978), Geologic map of the Coprates quadrangle of Mars (MC-18), scale 1:5,000,000, *U.S. Geol. Surv. Misc. Invest. Ser., Map I-897*.
McCauley, J. F., M. H. Carr, J. A. Cutts, W. K. Hartmann, H. Masursky, D. J. Milton, R. P. Sharp, and D. E. Wilhelms (1972), Preliminary Mariner 9 report on the geology of Mars, *Icarus*, *17*, 289–327.
McEwen, A. S. (1989), Mobility of large rock avalanches: Evidence from Valles Marineris, Mars, *Geology*, *17*, 1111–1114.
McEwen, A. S., and M. C. Malin (1998), Layering in the upper crust of Mars seen in Valles Marineris by the Mars Orbital Camera, *Proc. Lunar Planet. Sci. Conf. 29th*, abstract 1908.
McGovern, P. J., S. C. Solomon, D. E. Smith, M. T. Zuber, M. Simons, M. A. Wieczorek, R. J. Phillips, G. A. Neumann, O. Aharonson, and J. W. Head (2002), Localized gravity/topography admittance and correlation spectra on Mars: Implications for regional and global evolution, *J. Geophys. Res.*, *107*(E12), 5136, doi:10.1029/2002JE001854.
Mège, D., and D. Gatineau (2003), Valles Marineris wallslopes: Evidence for Amazonian variations in wallrock strength and oblique crustal fabric, *Proc. Lunar Planet. Sci. Conf. 34th*, abstract 1748.
Mège, D., and P. Masson (1996), A plume tectonics model for the Tharsis province, *Planet. Space Sci.*, *44*, 1499–1546.
Mellon, M. T., B. M. Jakosky, and S. E. Postawko (1997), The persistence of equatorial ground ice on Mars, *J. Geophys. Res.*, *102*(E8), 19,357–19,369.
Moore, J. M., M. T. Mellon, and A. P. Zent (1996), Mass wasting and ground collapse in terrains of volatile-rich deposits as a solar system-wide geological process: The pre-Gallileo view, *Icarus*, *122*, 63–78.
Peulvast, J.-P., D. Mège, J. Chiciak, F. M. Costard, and P. L. Masson (2001), Morphology, evolution and tectonics of Valles Marineris wall-slopes (Mars), *Geomorphology*, *37*, 329–352.
Phillips, R. J., C. D. Brown, S. A. Hauck, B. W. Harrington, M. A. Wieczorek, and J. W. Head (1998), Preliminary geomorphology results from the MGS MOLA experiment, *Proc. Lunar Planet. Sci. Conf. 29th*, abstract 1503.
Quantin, C., P. Allemand, and C. Delacourt (2003), Valles Marineris landslides: Morphologies, ages and dynamics, in *6th International Conference on Mars*, abstract 3053, Lunar and Planet. Inst., Houston, Tex.
Rossbacher, L. A., and S. Judson (1981), Ground ice on Mars: Inventory, distribution, and resulting landforms, *Icarus*, *45*, 39–59.
Rossi, A. P., G. Komatsu, and J. S. Kargel (2000), Rock glacier-like landforms in Valles Marineris, Mars, *Proc. Lunar Planet. Sci. Conf. 31st*, abstract 1587.
Sayles, F. H. (1966), Low temperature soil mechanics, technical note, Cold Regions Res. and Eng. Lab., U.S. Army Corps of Eng., Hanover, N. H.
Schultz, R. A. (1991), Structural development of Coprates Chasma and western Ophir Planum, Valles Marineris rift, Mars, *J. Geophys. Res.*, *96*(E5), 2777–2792.
Schultz, R. A. (1998), Multiple-process origin of Valles Marineris basins and troughs, Mars, *Planet. Space Sci.*, *46*, 827–834.
Schultz, R. A. (2002), Stability of rock slopes in Valles Marineris, Mars, *Geophys. Res. Lett.*, *29*(19), 1932, doi:10.1029/2002GL015728.
Selby, M. J. (1980), A rock mass strength classification for geomorphic purposes: With tests from Antarctica and New Zealand, *Zeitschr. Geomorphol.*, *24*, 31–51.
Sharp, R. P. (1973), Mars: Troughed terrain, *J. Geophys. Res.*, *78*, 4063–4072.
Squyres, S. W. (1978), Martian fretted terrain: Flow of erosional debris, *Icarus*, *34*, 600–613.
Squyres, S. W. (1989), Water on Mars, *Icarus*, *79*, 229–288.
Squyres, S. W., S. M. Clifford, R. O. Kuzmin, J. R. Zimbelman, and F. M. Costard (1992), Ice in the Martian regolith, in *Mars*, edited by H. H. Kieffer et al., pp. 523–554, Univ. of Ariz. Press, Tucson.
Sullivan, R. (1992), Weathering processes implied from analysis of small Martian avalanche chutes, in *Workshop on Chemical Weathering on Mars*, *LPI Tech. Rep. 92-04, 1*, pp. 36–37, Lunar and Planet. Inst., Houston, Tex.
Tanaka, K. L., and M. P. Golombek (1988), Martian tension fractures and the formation of grabens and collapse features at Valles Marineris, *Proc. Lunar Planet. Sci. Conf. 19th*, 383–396.
Tanaka, K. L., and D. J. MacKinnon (2000), Pseudokarst origin for Valles Marineris, *Proc. Lunar Planet. Sci. Conf. 31st*, abstract 1780.
Tsytovich, N. A. (1960), Bases and foundations on frozen soils, translated from Russian by L. Drashevska, *Highway Res. Board Spec. Rep. 58*, *Natl. Res. Counc. Publ. 804*, Natl. Acad. of Sci., Washington, D. C.
Whalley, W. B., and F. Azizi (2003), Rock glaciers and protalus landforms: Analogous forms and ice sources on Earth and Mars, *J. Geophys. Res.*, *108*(E4), 8032, doi:10.1029/2002JE001864.
Williams, J. P., and D. A. Paige (2002), Layered rocks of Valles Marineris: Layered intrusive rocks on Mars, *Proc. Lunar Planet. Sci. Conf. 33rd*, abstract 2058.
Williams, P. J., and M. W. Smith (1989), *The Frozen Earth: Fundamentals of Geocryology*, Cambridge Univ. Press, New York.

J. A. Jernsletten, 1917 Florida Drive, Seabrook, TX 77586-2985, USA. (joern@jernsletten.name)